DE GRUYTER
Z. Kristallogr. 2018; 233(9–10): 707–721

Simon Grabowsky*, Ole Mallow, Rumpa Pal, Yves Pergandé, Enno Lork, Christian Näther* and Jens Beckmann*

Conformational trimorphism of bis(2,6-dimesitylphenyl)ditelluride

https://doi.org/10.1515/zkri-2018-2077
Received February 19, 2018; accepted July 19, 2018; published online August 28, 2018

Abstract: Besides the previously known α-form (monoclinic, $P2_1/c$, Z = 4) of bis(2,6-dimesitylphenyl)ditelluride, two new polymorphic modifications, namely the β-form (monoclinic, $P2_1/c$, Z = 8) and the γ-form (triclinic, $P\bar{1}$, Z = 2), were obtained serendipitously during chemical reactions. In all three modifications, the individual molecules possess significantly different conformations and bond parameters, such as Te–Te bond lengths, C–Te–Te bond angles, C–Te–Te–C torsion angles and intramolecular Menshutkin interactions, which is also reflected in their non-covalent interactions with adjacent molecules in the crystal lattice via London dispersion and electrostatic forces. The interplay between intermolecular and intramolecular forces in these conformational polymorphs was investigated using quantum chemical calculations, which reveal that the β-form should be thermodynamically stable at absolute zero. In contrast, crystallization experiments and thermoanalytical investigations indicate that the α-form is stable at high temperatures and therefore, both forms might be related by enantiotropism.

Keywords: conformational polymorphism; crystal modifications; crystal packing; London dispersion; tellurium.

***Corresponding authors: Simon Grabowsky and Jens Beckmann,** Institut für Anorganische Chemie und Kristallographie, Universität Bremen, Leobener Straße 3 und 7, 28359 Bremen, Germany, E-mail: simon.grabowsky@uni-bremen.de (S. Grabowsky); j.beckmann@uni-bremen.de (J. Beckmann); and
Christian Näther, Institut für Anorganische Chemie, Christian-Albrechts-Universität zu Kiel, Max-Eyth-Str. 2, 24118 Kiel, Germany, E-mail: cnaether@ac.uni-kiel.de
Ole Mallow, Rumpa Pal, Yves Pergandé and Enno Lork: Institut für Anorganische Chemie und Kristallographie, Universität Bremen, Leobener Straße 3 und 7, 28359 Bremen, Germany

Introduction

The lattice energy of molecular crystals is dominated by intermolecular non-covalent forces. These forces include electrostatic interactions between permanent multipoles, induced and/or polarization interactions between permanent and induced multipoles as well as London dispersion interactions between instantaneous and induced multipoles [1–3]. It is debated whether these forces give rise to the formation of atom···atom bonds between molecules in crystals, such as hydrogen and halogen bonds or metallophilic interactions, or whether they should be considered as globally acting forces between pairs of molecules [4–7]. Hydrogen bonds as strong intermolecular interactions dominated by electrostatics can more directly be related to directed atom···atom contacts, whereas London dispersion interactions are weaker and less directed [8]. In this context, the claim of the discovery of hydrogen–hydrogen bonds as a new class of stabilizing intermolecular bonding [9] was disputed [10]. Certainly, intermolecular London dispersion forces governed by multiple hydrogen–hydrogen contacts are "subtle, but not faint" [11], and have recently shown to give rise to a remarkably short intermolecular hydrocarbon H···H distance [12].

London dispersion forces are also structure determining for intramolecular geometries and molecular conformations. In recent years, many examples have been published that show the high significance of London dispersion for molecular chemistry and structure [13–17]. The energy associated with conformational changes has an influence on the lattice energy of molecular crystals and vice versa. If the same molecular compound crystallizes in different polymorphs comprised of different conformers, this is called *conformational polymorphism* [18, 19]. The relative orientation of the molecules in the crystal lattice is related to the type and strength of the intermolecular non-covalent forces [20–23]. Hence, the interplay of inter- and intra molecular forces for the formation of conformational polymorphs must be assessed. In the absence of hydrogen bonding or any other stronger non-covalent force, the role of London dispersion acting via different intra- and inter

molecular arrangements may be evaluated to improve the understanding of packing or crystal field effects. Already in 1970, Kitaigorodskii suggested a strategy to investigate the role of the crystalline field on the molecular conformation [24, 25], which can be summarized within four steps [18]:

1. comparison of the structure of gaseous and crystalline molecules,
2. comparison of geometries of crystallographically independent molecules in the same crystal,
3. analysis of the structure of a molecule whose crystallographic symmetry is lower than its free molecule symmetry,
4. comparison of the conformation of molecules in different polymorphic modifications.

The Hirshfeld surface analysis is a rather new powerful tool to unravel intermolecular non-covalent forces in molecular crystals [26–28], particularly in the context of polymorphism [22, 29, 30], which will be connected with Kitaigorodskii's criteria in this study. Here, we analyze the conformational polymorphs of bis(2,6-mesitylphenyl) ditelluride, $(2,6\text{-}Mes_2C_6H_3Te)_2$, that occurs in three different crystalline modifications containing a total of four independent conformers (Scheme 1). This compound is characterized by bulky meta-terphenyl substituents that engage in intramolecular Menshutkin type interactions [31–34]. It has been previously used as the starting material for the preparation of novel compound classes including mixed-valent tellurenyl halides [35], base-supported tellurenyl cations [36], tellurinic [37] and telluronic acids [38], as well as ditelluride radical cations [39]. During the work with $(2,6\text{-}Mes_2C_6H_3Te)_2$, two of these polymorphs were found serendipitously and are reported here for the first time.

In this context, it is noted that conformational polymorphism is not uncommon in tellurium chemistry [40]. There are three pairs of polymorphic diarylditellurides, namely, bis(2-naphthyl)ditelluride [41], bis(4-chlorophenyl)ditelluride [42, 43] and bis(4-tolyl)ditelluride [44, 45], which differ for example in their C–Te–Te–C torsion angles.

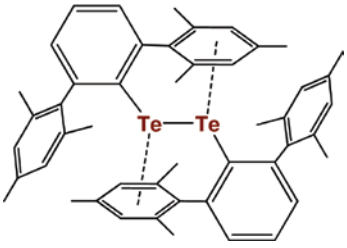

Scheme 1: Lewis formula representation of bis(2,6-dimesitylphenyl) ditelluride illustrating the intramolecular Menshutkin interactions.

Results and discussion

Crystallization

Bis(2,6-dimesitylphenyl)ditelluride, $(2,6\text{-}Mes_2C_6H_3Te)_2$, was obtained as previously described [35]. Following the published procedure, the α-form was obtained in bulk after crystallization from hexane, which was unambiguously confirmed by X-ray powder diffraction (XRPD). The experimental powder trace closely matched the theoretical pattern calculated from the published single crystal X-ray data (Figure 1) [35].

Meanwhile, two more modifications, denoted the β-form and the γ-form, were obtained by serendipitous crystallization from reaction mixtures containing $(2,6\text{-}Mes_2C_6H_3Te)_2$ and investigated by single crystal X-ray diffraction. The crystal and refinement data of all three modifications are collected in Table 1. The packing diagrams of all three polymorphic modifications are shown in Figure 2. The β-form crystallized at room temperature from acetonitrile during an attempt to prepare the radical cation $[(2,6\text{-}Mes_2C_6H_3Te)_2]^+$ from $(2,6\text{-}Mes_2C_6H_3Te)_2$ and $NO(SO_3SCF_3)$ [39]. The γ-form was obtained at room temperature from the redox reaction between $2,6\text{-}Mes_2C_6H_3TeCl_3$ and $Fe(CO)_5$ in ether/hexane, which gave rise to the formation of $(2,6\text{-}Mes_2C_6H_3Te)_2$, $FeCl_2$ and CO. All attempts to obtain the β-form and the γ-form by recrystallization of the α-form from acetonitrile, ether/hexane or other solvents, such as dichloromethane or

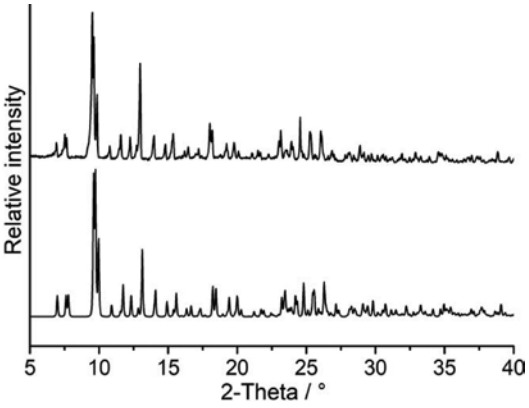

Fig. 1: Experimental XRPD pattern of the α-form obtained by the published procedure (top) and calculated XRPD pattern from the single crystal data of the α-form (bottom).

Tab. 1: Crystal data and structure refinement of α-, β- and γ-form of $(2,6\text{-Mes}_2C_6H_3Te)_2$.

	α-form [35]	β-form	γ-form
Formula	$C_{48}H_{50}Te_2$	$C_{48}H_{50}Te_2$	$C_{48}H_{50}Te_2$
Formula weight, g mol^{-1}	882.08	882.08	882.08
Crystal system	monoclinic	monoclinic	triclinic
Crystal size, mm	0.19×0.15×0.13	0.40×0.30×0.30	0.50×0.10×0.05
Space group, Z (Z')	$P2_1/c$, 4 (1)	$P2_1/c$, 8 (2)	$P\bar{1}$, 2 (1)
a, Å	11.518(2)	22.3331(6)	11.105(2)
b, Å	15.092(2)	16.9611(5)	12.123(4)
c, Å	23.556(3)	21.9580(6)	16.775(2)
α, °	90	90	100.27(1)
β, °	99.388(3)	102.778(2)	109.15(1)
γ, °	90	90	97.94(2)
V, Å^3	4039.8(9)	8111.6(4)	2051.7(8)
Temperature, K	173	173	173
Void volume,[a] Å^3	591.6	1179.3	309.9
Percentage of voids	14.6%	14.5%	15.1%
ρ_{calcd}, mg m^{-3}	1.450	1.470	1.428
μ (Mo $K\alpha$), mm^{-1}	1.476	1.445	1.453
F(000)	1768	3536	884
θ range, deg	1.87–25.89	2.22–25.50	2.55–27.50
Index ranges	$-16 \le h \le 16$	$-24 \le h \le 24$	$-7 \le h \le 14$
	$-21 \le k \le 19$	$-20 \le k \le 20$	$-15 \le k \le 15$
	$-33 \le l \le 28$	$-26 \le l \le 26$	$-21 \le l \le 21$
No. of reflns collected	49,701	440,071	10,990
Completeness to θ_{max}	99.6%	98.9%	99.5%
No. indep. reflns	12,323	14,908	9368
No. obsd reflns with [$I > 2\sigma(I)$]	8172	11,726	5550
No. refined params	451	925	463
GooF (F^2)	0.972	1.285	0.960
R_1 (F) [$I > 2\sigma(I)$]	0.0433	0.0472	0.0649
wR_2 (F^2) (all data)	0.1186	0.1139	0.1776
Largest diff peak/hole, e Å^{-3}	1.431/−1.579	1.743/−0.887	1.605/−1.870
CCDC number	651206	1823140	1823141

[a]Calculated using Crystal Explorer and a 0.0003 a.u. isodensity surface [46].

chloroform, were unsuccessful. Problems in repeatedly preparing known polymorphs have been previously recognized and addressed with the term 'disappearing polymorphs' [47, 48].

Thermoanalysis of the α-form and thermodynamic considerations

The thermal properties of the α-form were investigated using simultaneously differential thermoanalysis and thermogravimetry (DTA-TG), differential scanning calorimetry (DSC) and X-ray powder diffraction to check if a transformation into the β-form and the γ-form can be observed. The calculated X-ray powder patterns of all three forms turned out to show distinctive features, which could be used to distinguish them unambiguously (Figure S1). DSC measurements of the α-form show an endothermic event at an onset temperature T_o of 283 °C that corresponds to the melting point of this compound (Figure 3).

Upon cooling, super cooling was observed and the melt solidified at about 241 °C. There are no hints for any further polymorphic transformation of the α-form. If the residue obtained by cooling of the melt was investigated by XRPD it was proven that the α-form is obtained exclusively (Figure S2). Heating rate dependent DSC measurements showed a similar behavior and again no evidence for a polymorphic phase transition was found (Figure S3). To check the reversibility of melting, several heating and cooling cycles were measured by DSC, which clearly shows that the heat of fusion as well as the heat of crystallization decreases dramatically when the sample is melted and recrystallized several times (Figure 4 and Table 2).

Five different DSC measurements with the α-form at 10 °C/min were carried out to determine the melting temperature and the heat of fusion more precisely (Table S1).

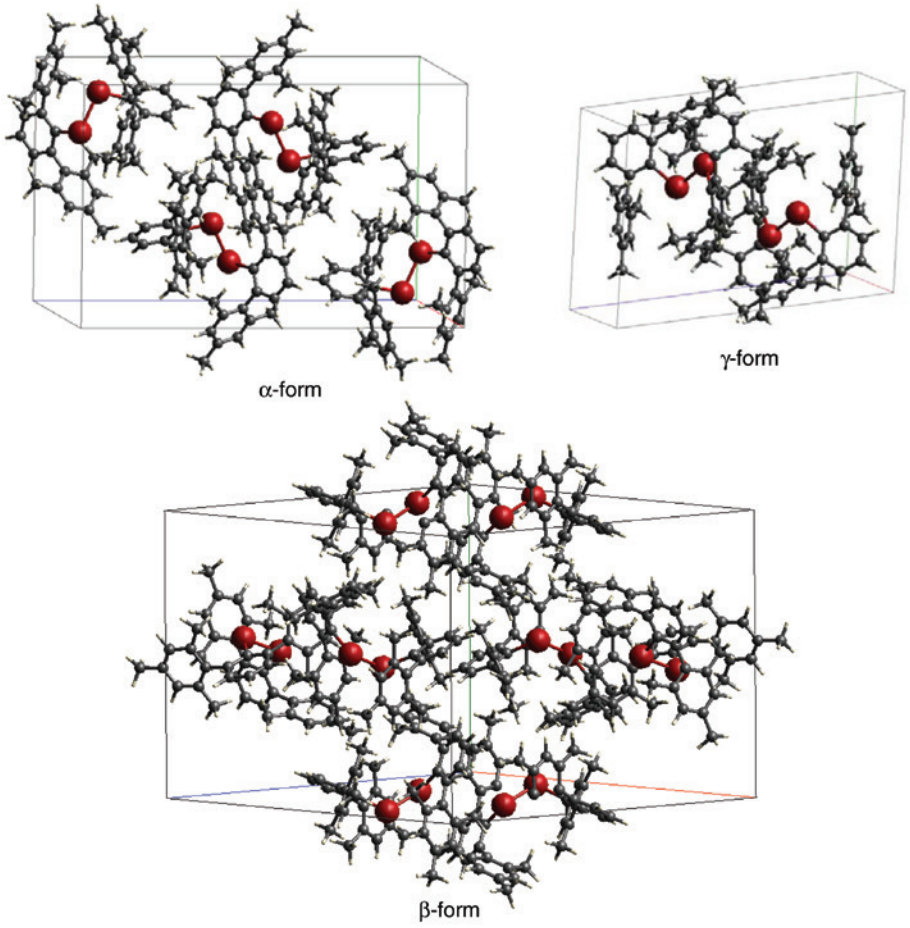

Fig. 2: Unit cell representations of the a α-form (left), β-form (bottom) and γ-form (right) of (2,6-$Mes_2C_6H_3Te)_2$ showing the packing of the appropriate number (Z) of complete molecules.

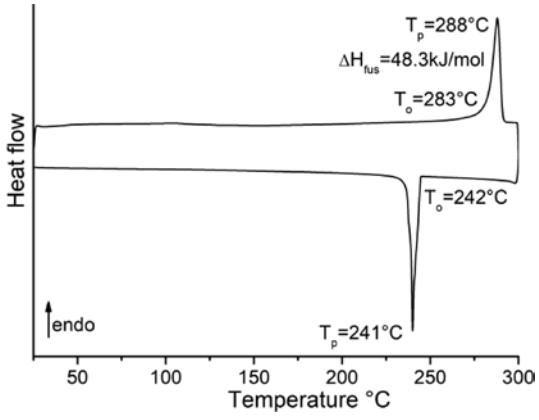

Fig. 3: DSC curve of the α-form at 10 °C/min. Given are the peak (T_p) and onset (T_o) temperatures as well as the heat of fusion.

The average values are $T_o = 280\,°C$, $T_p = 286\,°C$ and $\Delta H_{fus} = 46.8$ kJ/mol. Moreover, after the first melting the melting temperature decreases by about 30 °C indicating thermal decomposition of the material and the melting peak becomes very broad. If the residue obtained after the tenths cycle was investigated by XRPD it was obvious that a part of the sample had been transformed into elemental tellurium (Figure S4). When the DSC measurements were repeated and 20 heating and cooling cycles were measured, the whole sample transformed into elemental tellurium (Figures S5 and S6). DTA-TG measurements of the α-form under nitrogen atmosphere showed melting at 290 °C, which was followed by a strong decrease of the sample mass at about 372 °C, which corresponds to the decomposition of the material (Figure 5). Upon further heating a third endothermic event was observed at 449 °C, which exactly corresponds to the melting point of elemental tellurium. A closer look at the TG curve reveals that the sample mass decreases slightly below the melting point, which can originate from sublimation or decomposition of this modification (Figure 5). A further DTA-TG measurement in air atmosphere shows no oxidation of the α-form below the melting point (Figure S7). Finally, the α-form was annealed below the melting point at 250 °C for 48 h

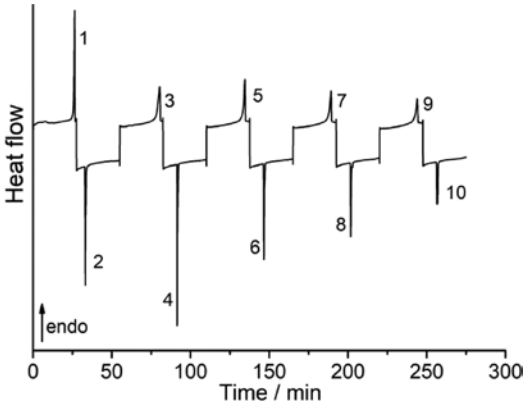

Fig. 4: DSC heating and cooling cycles of the α-form at 10 °C/min (For the peak and onset temperatures as well as the heat of fusion or crystallization see Table 2).

Tab. 2: Results of the DSC runs using several heating and cooling cycles at 10 °C/min.

No	Comment	T_p	T_o	ΔH_{fus}
1	1. heating	288	285	55.1
2	1. cooling	244	246	−43.6
3	2. heating	279	276	50.7
4	2. cooling	209	210	−38.7
5	3. heating	270	266	46.5
6	3. cooling	209	211	−34.5
7	4. heating	267	264	42.6
8	4. cooling	208.1	210	−28.9
9	5. heating	264	260	36.7
10	5. cooling	208	212	−26.8

T in °C, ΔH_{fus} in kJ/mol.

and afterwards investigated by XRPD. This experiment clearly shows that the residue consists of the α-form exclusively, which also indicates that this form might be thermodynamically stable at high temperatures (Figure S8).

From all investigations mentioned above, there is no indication that the α-form can be converted into one of the serendipitously obtained forms. From this point of view, it appears likely that the α-form represents the thermodynamically stable form, at least between room-temperature and the melting point. However, it is noted that the density of the α-form ($\rho = 1.450$ mg m^{-3}) is significantly lower than that of the β-form ($\rho = 1.470$ mg m^{-3}), which according to the density rule indicates that the latter is thermodynamically stable at low temperatures [25, 49]. Usually it is argued that the highest density correlates with a maximum of vander-Waals interactions and that it is therefore found in the most stable form of a given set of polymorphs at absolute zero where the entropy plays no role [25, 49]. The trend in crystal densities agrees well with the trend in crystal voids (Table 1), which are most pronounced in the γ-form with

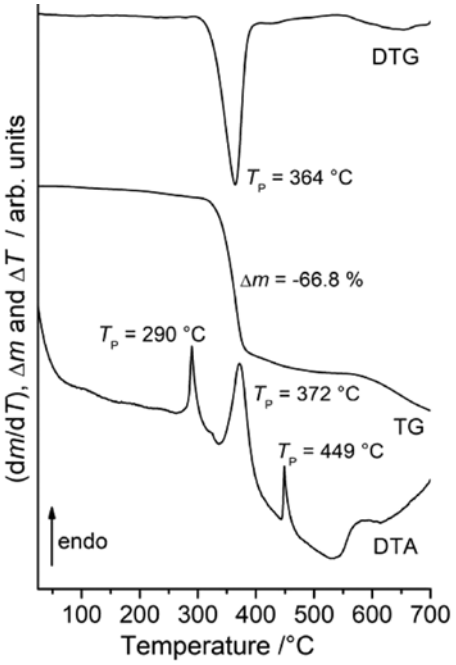

Fig. 5: DTG, TG and DTA curve of the α-form (Heating rate: 8 °C/min; nitrogen atmosphere). Given are the peak temperatures (T_p) in °C and the mass loss in %.

the lowest density and are least pronounced in the β-form, which has the highest density.

If the above experimental findings are interpreted in a thermodynamic way, it is likely that the free energy temperature curves of the α- and the β-form will cross somewhere below room-temperature. Therefore, both modifications seem to be related by enantiotropism. In this case, one would expect an endothermic phase transition of the β- into the α-form upon heating. To prove these assumptions, a sample of the β-form would be needed and because this form might be metastable at room-temperature we tried to obtain it under kinetic control. Therefore, the α-form was dissolved in dichloromethane and afterwards the solvent was removed immediately under vacuum. However, if the residue is investigated by XRPD, the α-form was obtained exclusively (Figure S9). Attempts to obtain a different form by sublimation at different temperatures were also undertaken, however, even after 1 week only a few milligrams of a residue were obtained, which turned out to be amorphous against X-rays.

Intramolecular bonding and conformational analysis

The availability of three crystal modifications of $(2,6\text{-Mes}_2C_6H_3Te)_2$ meets the 4th criterion proposed by

Kitaigorodskii (see above) [18]. The β-form shows two crystallographically independent conformers in the unit cell, which fulfills Kitaigorodskii's 2nd criterion (see above) [18]. The molecular structures of the four crystallographically independent conformers of the α-, β- and γ-form are shown in Figure 6 and selected bond parameters are collected in Table 3. The Te–Te bond lengths of the two conformers of the β-form (2.700(1), 2.705(1) Å) are somewhat shorter than those of the α-form (2.711(1) Å) and the γ-form (2.712(1) Å). The C–Te–Te bond angles are indifferent and vary in a small range from 100.1(2)° to 104.4(2)°. The torsion angles span a larger range between –112.2(3)° and –134.4(3)° and are therefore used as descriptors throughout the discussion characterizing the conformers.

Notably, all of these torsion angles are significantly larger than those of other diaryldditellurides, such as $(PhTe)_2$ (–90.5(2)°) [50] and (2,4,6-*t*-$Bu_3C_6H_2Te)_2$ (92.2(3)°) [51], regardless of the steric demand of the organic substituents and probably due to the presence of intramolecular Menshutkin interactions between the Te atoms and the π electrons of the mesityl groups. Such interactions have been the subject of a survey of the crystallographic literature [32, 33] as well as of theoretical studies [52]. The comparison of all three forms regarding the C–Te–Te–C torsion angles and regarding the occurrence of short Menshutkin interactions shows resemblances between two pairs of conformers: On the one hand, the two conformers of the β-form are very similar, in having small C–Te–Te–C torsion angles (–113.2(2)° and –112.2(3)°) and rather long Menshutkin interactions (3.736(1)–3.990(2) Å). On the other hand, the conformers of the α-form and of the γ-form resemble each other in the large C–Te–Te–C torsion angles (–123.1(1)° and –134.4(3)°) and one (3.382(3) Å) or two (3.382(2) and 3.482(2) Å) rather short Menshutkin interactions. The shorter Menshutkin interactions are associated with Cg–Te–Te angles that are between 90.1(1) and 92.2(1)°, whereas the longer Menshutkin interactions are related with Cg–Te–Te angles between 76.8(1) and 80.2(1)°.

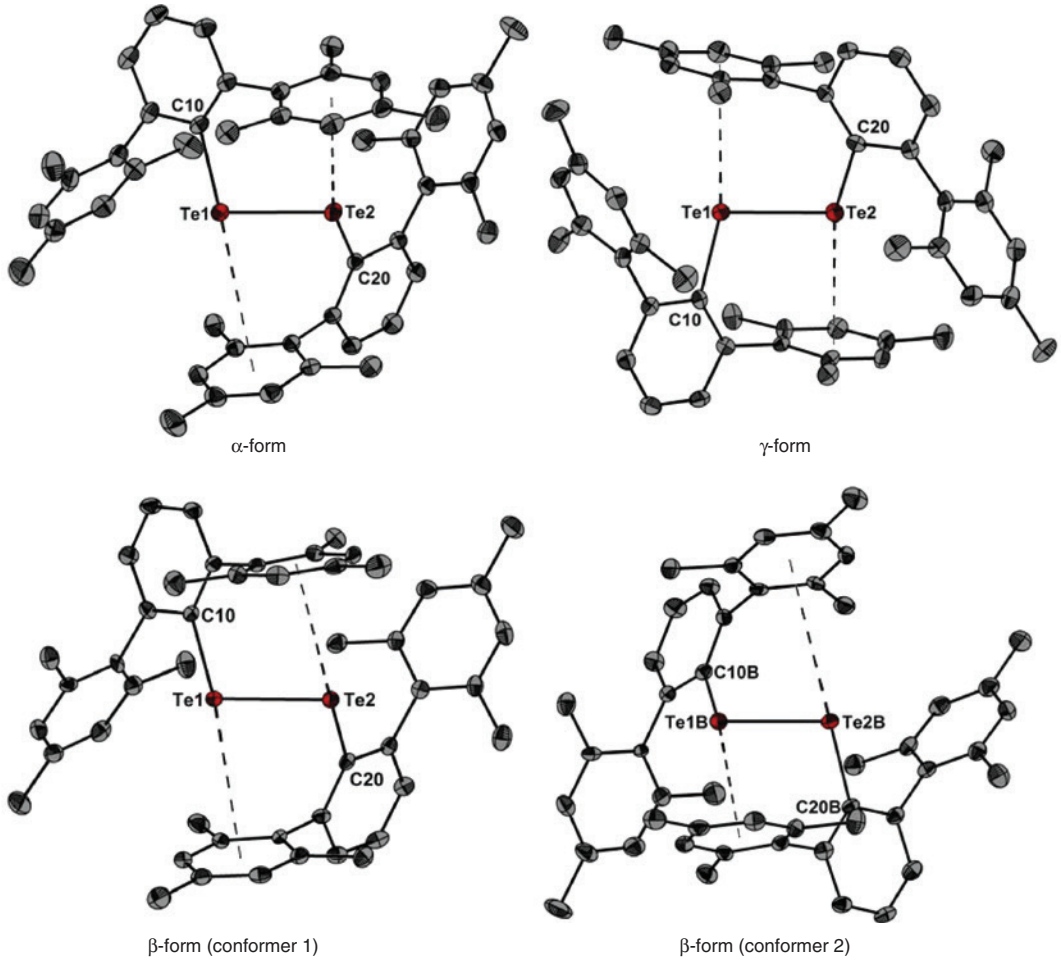

Fig. 6: Molecular structures of the four crystallographically independent conformers of $(2,6\text{-}Mes_2C_6H_3Te)_2$ showing 30% probability ellipsoids.

Tab. 3: Selected bond parameters of the four experimental conformers and the (partially) optimized conformers of $(2,6\text{-}Mes_2C_6H_3Te)_2$.

		α-form	β-form	γ-form
Experimental results from crystal structures				
d(Te–Te) in Å		2.711(1)	2.705(1)[a]	2.712(1)
			2.700(1)[b]	
C–Te–Te in °		103.0(1)	102.5(2), 103.8(2)[a]	100.1(2)
		103.2(1)	102.2(2), 104.4(2)[b]	104.2(2)
C–Te–Te–C in °		−123.1(1)	−113.2(2)[a]	−134.4(3)
			−112.2(3)[b]	
d(Cg–Te) in Å		3.382(3)	3.736(1), 3.905(1)[a]	3.382(2)
		3.844(5)	3.798(4), 3.990(2)[b]	3.482(2)
Cg–Te–Te in °		90.1(1)	76.3(1), 80.2(1) [a]	90.2(1)
		78.0(1)	75.8(1), 78.4(1)[b]	92.1(1)
Theoretical results from geometry optimization				
d(Te–Te) in Å	2.735[c]	2.725[d]	2.712[d]	2.735[d]
C–Te–Te in °	2×100.7[c]	2×102.2[d]	2×104.1[d]	2×100.7[d]
C–Te–Te–C in °	−134.3[c]	−123.1[d]	−113.2[d]	−134.4[d]
d(Cg–Te) in Å	2×3.254[c]	2×3.301[d]	2×3.346[d]	2×3.254[d]

[a]Conformer 1, [b]conformer 2, [c]full geometry optimization, [d]relaxed geometry optimizations with fixed C–Te–Te–C torsion angles.
All theoretical results shown include Grimme-type D3BJ empirical dispersion correction.

Importance of London dispersion and Menshutkin interactions

In an effort to meet Kitaigorodskii's 1st criterion [18] and to examine the conformational space in the gas phase, a full geometry optimization of $(2,6\text{-}Mes_2C_6H_3Te)_2$ was carried out with and without dispersion correction (empirical GD3BJ) starting from the experimentally observed geometries of the three modifications, which, however, had no influence on the found minimum. Without dispersion correction, the optimization settled in a minimum characterized by a C–Te–Te–C torsion angle of –126.3°, which is close to that observed in the experimental α-form (3.2° difference). Compared to that, the calculated Te–Te distance (2.750 Å) is 0.039 Å longer, and the Menshutkin interactions are less significant (Te···Cg: 3.814/3.815 Å vs. 3.382(3), 3.844(5) Å). The results with dispersion correction are listed in Table 3. Here, the optimization settled in a minimum characterized by a C–Te–Te–C torsion angle of –134.4°, which closely resembles that observed in the experimental γ-form (0.1° difference). Compared to that form, the calculated Te–Te bond length (2.735 Å) is by 0.023 Å longer, whereas the Menshutkin interactions are more significant (Te···Cg: 2×3.254 Å vs. 3.382(2), 3.482(2) Å). The difference in the molecular energies between the molecular structures calculated with and without dispersion correction is –847.85 kJ mol^{-1}, which emphasizes the large influence of London dispersion on the molecular geometry. Notably, all calculated gas phase structures are more symmetric than the experimentally established conformers, particularly when the Menshutkin interactions are considered, which fulfils Kitaigorodskii's 3rd criterion [18].

In an effort to illustrate the influence of the dispersion on the topology of the electron density, Atoms in Molecules (AIM) [53] bond paths and the non-covalent interaction (NCI) index [54, 55] were calculated (Figure 7). Besides the expected bond paths for the primary bonds defining the atomic connectivity, there is a varying number of intramolecular bond paths related to dispersive and electrostatic interactions. In both cases, AIM indicates one Te···C contact for each Te atom related to interactions with mesityl groups. In the dispersion-corrected structure, there are also two Te···H contacts for each Te atom arising from interactions with the methyl groups. Complementary to the AIM topology, the NCI shows more prominent contact areas between mesityl groups and the Te atoms for the geometry obtained with dispersion correction. Hereafter, dispersion correction is applied throughout the rest of the manuscript (Table 3).

In an effort to visualize the shape, size and spatial orientation of the lone pairs at the Te atoms, the electron localizability indicator (ELI-D) [56, 57] was calculated (Figure 8). As expected for the oxidation state +I, each Te atom displays two lone pairs, which are situated perpendicularly to the planes defined by the Te atoms and the central aromatic rings. In this way, the lone pairs occupy space between the Te atoms and the flanking mesityl groups that engage in the Menshutkin interactions.

It is noteworthy, that the inclusion of a continuum solvation model (COSMO) [58] with MeCN into the

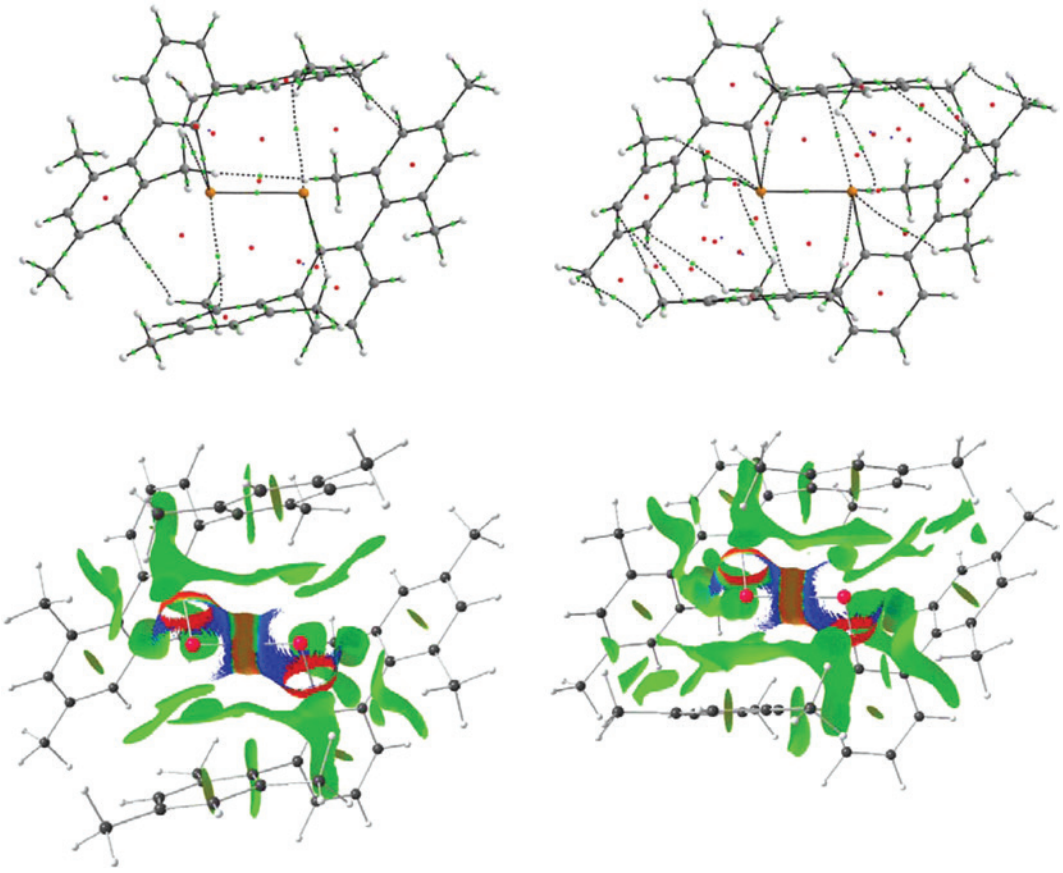

Fig. 7: Atoms in Molecules (AIM) molecular graphs showing bond paths and critical points (green = bond critical points, red = ring critical points, blue = cage critical points) (top) and non-covalent interaction (NCI) index (bottom) of the full geometry optimized (2,6-$Mes_2C_6H_3Te)_2$ without (left) and with (right) dispersion correction. The NCI plots are at an isosurface of 0.5 a.u. of the reduced density gradient, with the sign of the second eigenvalue of the electron-density Hessian Matrix (λ_2) multiplied with the electron density plotted onto it. The color scale is from −0.05 (blue, attractive) to +0.05 a.u. (red, repulsive).

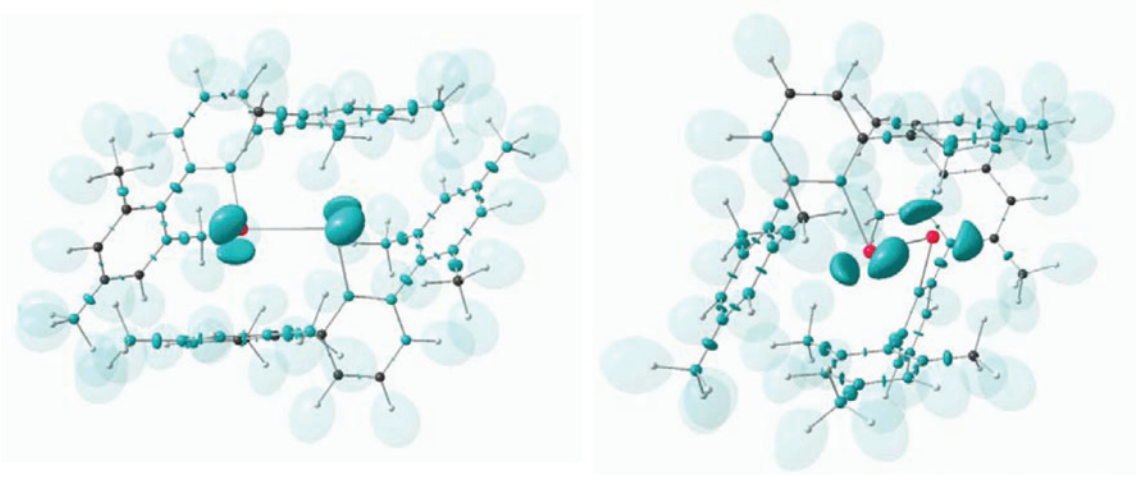

Fig. 8: Two orientations of the electron localizability indicator (ELI-D) visualizing the size, shape and spatial orientation of the Te lone pairs of the fully geometry optimized (2,6-$Mes_2C_6H_3Te)_2$ upon applying dispersion correction using an isovalue of 1.85.

optimization had only a marginal effect on the minimum structure, e.g. it only changed the C–Te–Te–C torsion angle from –134.4° to –137.1°.

Relative molecular and cohesive energies

Besides the full geometry optimization, relaxed geometry optimization with torsion angles restrained to –123.1° (α-form), –113.2° (conformer 1 of the β-form) and –134.4° (γ-form) were carried out (Table 3). In addition, a relaxed potential energy surface scan was conducted using Me_2Te_2 as a simple model compound, whereby the C–Te–Te–C torsion was varied in 5° steps between 60° and 180° (Figure 9). In most experimentally observed diarylditellurides, the absolute C–Te–Te–C torsion angles scatter around 90° (see also discussion above), which is consistent with the minimum C–Te–Te–C torsion angle (88.3°) found for MeTeTeMe. Going to larger C–Te–Te–C torsion angles, the relative energy steadily increases to a maximum of 25.62 kJ mol^{-1} at 180°. Compared to this energy profile, the relative energies of isolated conformers with optimized geometries at restrained C–Te–Te–C angles show a reverse trend: The restrained conformer presenting the β-form (–113.2°) shows the highest relative energy with 8.38 kJ mol^{-1}, followed by the α-form (–123.1°) with 2.23 kJ mol^{-1}, whereas the γ-form (–134.4°) is close to the minimum (Table 4). In the same order, the Menshutkin interactions become more significant: the restrained conformer presenting the β-form (–113.2°) shows the longest Te···Cg distance with 3.346 Å, followed by the α-form (–123.1°) with 3.301 Å and finally the γ-form (–134.4°) with 3.254 Å. These observations allow the conclusion that the energy loss associated with increasing C–Te–Te–C torsion angles are compensated by strengthening of the Menshutkin interactions.

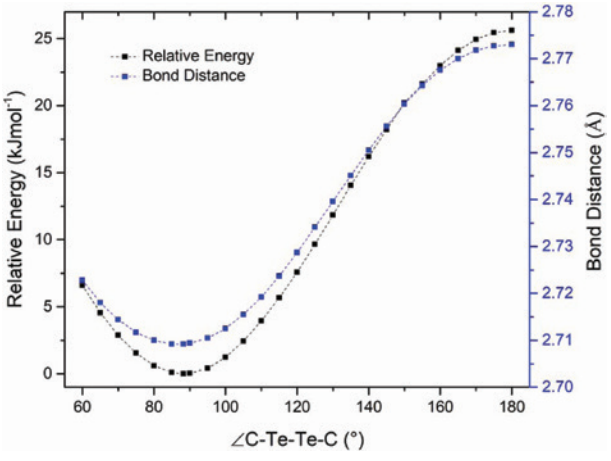

Fig. 9: Relaxed potential energy surface scan of Me_2Te_2 with fixed C–Te–Te–C torsion angles from 60° to 180° in 5° steps.

Tab. 4: Relative energies of the isolated conformers with optimized geometry at fixed C–Te–Te–C angles and with experimental geometries, relative energies of the unit cells per molecules as well as absolute and relative cohesive energies, in kJ mol^{-1}.

	α-form	β-form	γ-form
Relative energy of the isolated conformers with optimized geometry at fixed C–Te–Te–C angle[c,d]	2.23	8.38	<0.01
Relative energy of unit cell per molecule[e]	45.07	0	34.76
Relative energy of the isolated conformers with experimental geometry[e]	17.05	0.41[a] 0[b]	7.77
Absolute cohesive energy[e]	–187.56	–206.19[a] –205.85[b]	–191.40
Relative cohesive energy[e]	18.63	0[a] 0.34[b]	14.79
Estimated absolute cohesive energy[f]	–205.3	–215.4[a] –213.9[b]	–203.7
Estimated relative cohesive energy[f]	10.1	0[a] 1.5[b]	11.7

[a]Conformer 1, [b]conformer 2, [c]the energy of the freely optimized structure was set to 0 kJ mol^{-1}. [d]Calculated with Gaussian09, [e]calculated with Crystal14 under full periodic-boundary conditions, and taking basis-set superposition errors (BSSE) into account, [f]calculated with Crystral Explorer 17.

The total energies in the solid state calculated under fully periodic conditions include both intramolecular covalent bonding energies and intermolecular interactions energies (Table 4). With values of 45.07 and 34.76 kJ mol^{-1} relative to the lowest-energy modification β (0 kJ mol^{-1}), the energy differences are rather small, which is expected for polymorphic modifications. If the experimental conformers are extracted from the solid-state and taken into isolation, the resulting relative energies of the isolated conformers with experimental geometry show that the conformation of the molecules in the β-form are still energetically favored with only 7.77 and 17.05 kJ mol^{-1} energy difference to the conformations present in the α-form and γ-form. The absolute intramolecular energies calculated in the isolated state are responsible for over 99.99% of the total solid-state energies (about 6.3 GJ mol^{-1} per molecule in the unit cell). The cohesive energies (pure intermolecular interaction energies) ranging from 187.56 to 206.19 kJ mol^{-1} are much higher than the energy differences between the conformers and can thus stabilize unusual C–Te–Te–C torsion angles in the solid-state.

Again, the β-form is favored in terms of the cohesive energy.

Model energy estimation of cohesive energies

The solid-state periodic-boundary calculations at a high level of theory carried out here are the most accurate calculations possible with standard computer clusters for such big molecules with heavy elements. They still took about 1 month per calculation with our equipment. In contrast, the method of CrystalExplorer (CE) model energies introduced recently [59, 60] provides accurate and efficient dimer energies of intermolecular interactions within a few hours. The sum of all dimeric intermolecular interaction energies of the first shell of coordination around a central molecule in the crystal can serve as a first estimate for the cohesive energy of that molecule (second-last entry in Table 4). This procedure has been introduced in Ref. [61] and applied to a case of conformational polymorphism in Ref. [62].

The first coordination shell around the central molecule in the crystal of the α-form is shown in Figure 10. The central molecule is wrapped into its Hirshfeld surface [26, 63]. Different interaction partners are depicted in different colors, whereas the same interaction partners (same symmetry operation) have identical colors. Lists of all CE model energies and pictures of the interaction shells for all four independent molecules in the three crystalline polymorphic modifications are deposited in the Supplementary Material. The estimated cohesive energies are slightly more negative, and the relative differences smaller, compared to the calculated BSSE-corrected periodic-boundary cohesive energies. However, they show the same trends and are remarkably similar to the calculated ones if the drastic reduction in calculation time is considered. Hence, these accurate yet quickly estimated results allow delving more deeply into details of the intermolecular interaction patterns.

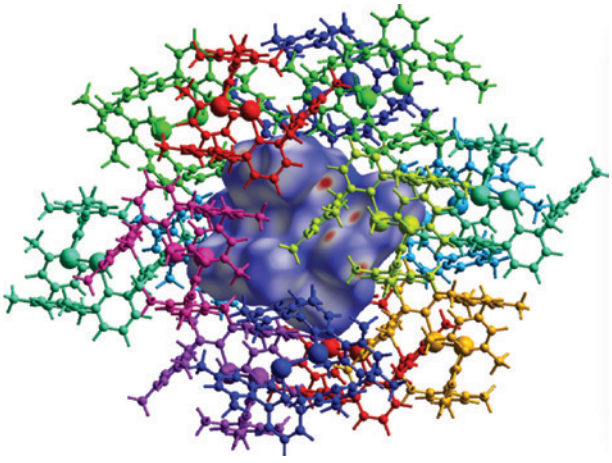

Fig. 10: Hirshfeld surface with the property d_{norm} mapped onto it (color code: −0.05 (red) to 1.75 (blue)) of the conformer of the α-form, surrounded by a cluster of molecules in the first interaction shell of the central molecule. A molecule is counted towards this first interaction shell if it has any atom within a radius of 3.8 Å to any atom of the central molecule.

Analysis of intermolecular interactions

Red spots on the Hirshfeld Surface (HS) that is color coded with the property d_{norm} [64] depict close atom–atom contacts, here hydrogen–hydrogen interactions. The percentages of all types of atom–atom contacts mediated through the HS, and the percentage of dispersion to the sum of the two energy forms dispersion and electrostatics (disregarding polarization and repulsion that need to be considered in addition for the total interaction energy) are given in Table 5 (see also Supplementary Material).

The H···H contacts and correspondingly London dispersion interactions dominate the crystal packing in all three compounds to approximately 80%. There are only small differences between the three modifications: dispersion contributions are less important in the α-form by about 3%, which corresponds to slightly more important electrostatic contributions that can be explained by a number of exceptionally short H···H distances in the α-form (visualized in Figure 11a) that do not occur in the two other forms. In the β-form, C···H contacts (representing C–H···π interactions, see Table 5) are most important,

Tab. 5: Percentage contributions of atom–atom interactions, and percentage contributions of dispersion to the sum of the attractive dispersion and Coulombic energies.

	α-form (%)	β-form (%)	γ-form (%)
H···H	83.4	80.1[a]	83.3
		81.4[b]	
C···H	14.8	16.9[a]	15.0
		16.0[b]	
Te···H	1.8	2.7[a]	1.6
		2.3[b]	
C···C	0.0	0.3[a]	0.1
		0.3[b]	
Dispersion	78.5	81.2[a]	81.4
		81.0[b]	

[a]Conformer 1, [b] conformer 2.

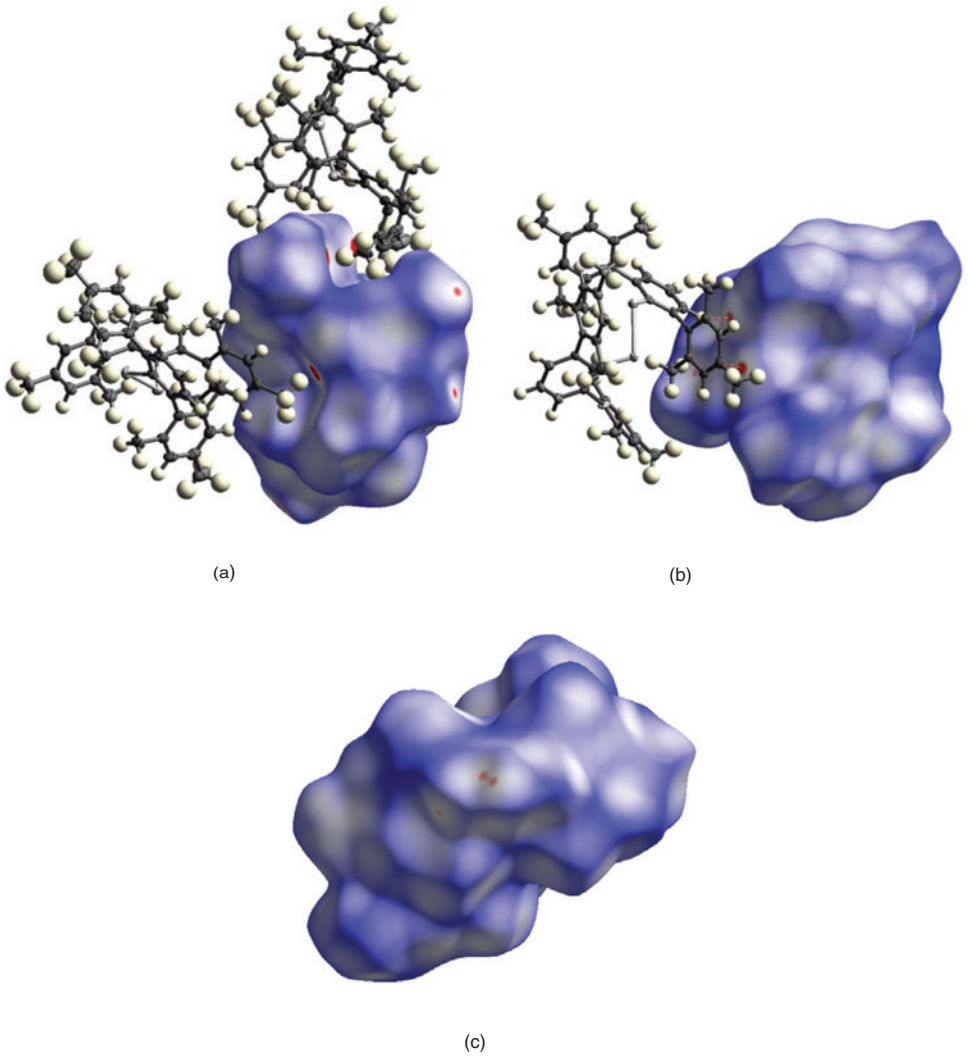

Fig. 11: Hirshfeld Surfaces of the conformer in the α-form (a), conformer 1 in the β-form (b) and the conformer in the γ-form (c). Significant interaction partners are shown if existent, d_{norm} mapped. Color code from −0.098 (red) to 0 (white) to 1.755.

and significant C–H···C short contacts in the β-form are visualized in Figure 11b. The γ-form exhibits very few contacts whose distances are smaller than the sum of the van der Waals radii of the atoms involved (Figure 11c).

The fingerprint plots in Figure 12 are a breakdown of all the HS-mediated close contacts onto a 2D picture plotting the distances of every surface point to the closest interior atom (d_i) against the distance to the closest exterior atom (d_e) [28]. The fingerprint plots confirm that the crystal packings in the three different polymorphs are significantly different from each other in terms of their overall shapes that allow a visual comparison of all intermolecular interactions at one glance (Figure 12). The plots show, as already implied in the previous paragraph and in Figure 11, that in the α-form there are many more short H···H contacts (central spike) than in the other forms, and the shortest of those (d_{min}(H···H) = 1.8 Å) are significantly shorter than the shortest H···H contacts in all other conformers in the other modifications (d_{min}(H···H) = 2.2 Å). These short H···H contacts are the manifestation of significantly attractive dispersion interactions with electrostatic contributions, see discussion above (see lists of individual dimeric energies in the Supplementary Material). Both conformers in the β-form have pronounced peripheral spikes representing C–H···π interactions with the closest C···H contacts being around 2.65 Å. Similar interactions do not exist in the other forms. The fingerprint plots for the two molecules in the asymmetric unit of the β-form are indeed slightly different confirming that they are independent molecules, but also being in line with the very small cohesive energy differences between them (Table 4).

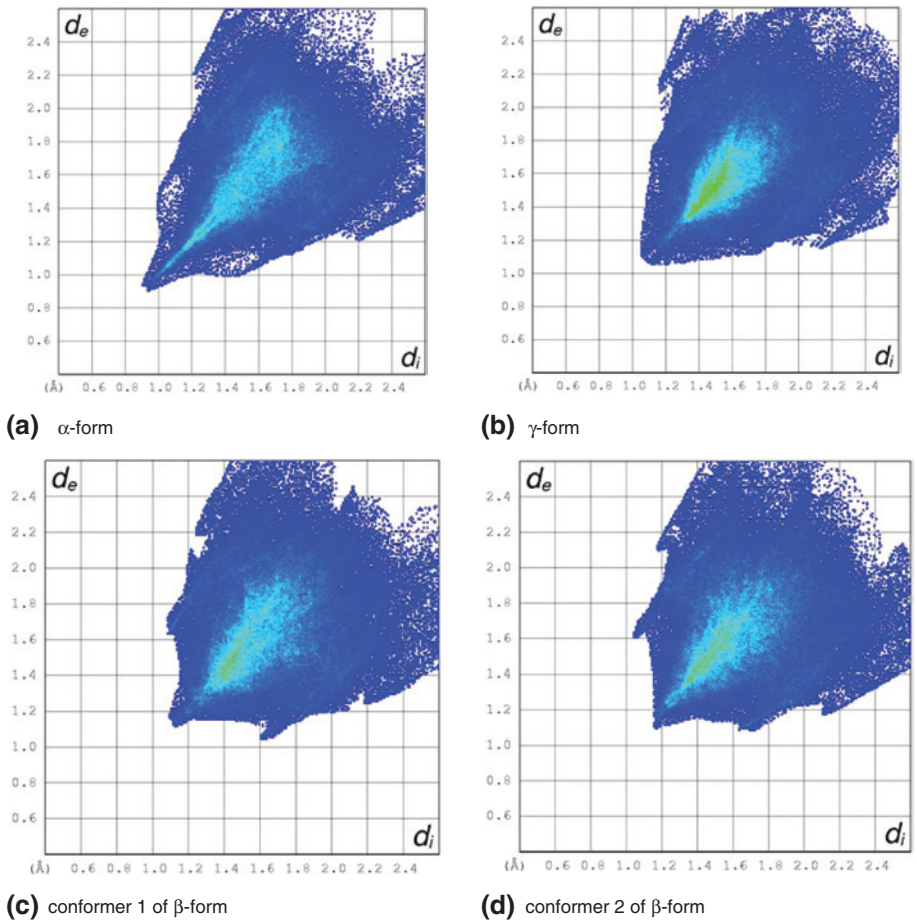

Fig. 12: Hirshfeld surface fingerprint plots.

Conclusion

Following along the suggested criteria of Kitaigorodskii [24, 25], we have investigated the interplay between the crystalline field and the molecular conformation of bis(2,6-dimesitylphenyl)ditelluride, $(2,6\text{-Mes}_2C_6H_3Te)_2$, that exists in three different polymorphs containing a total of four different conformers in the solid state. These conformers differ, amongst other parameters, in their C–Te–Te–C torsion angles and the strength of intramolecular Menshutkin interactions. The β-form shows the highest cohesive energy and since the entropy can be neglected at zero Kelvin [65] this corresponds to the lowest free energy. Therefore, it should represent the thermodynamic stable form at zero Kelvin. This is in nice agreement with the density rule [25] because the β-form shows the highest crystal density as well as the lowest percentage void volume in the crystal lattice, supporting the importance of high quality quantum chemical calculations. On the other hand, when the four independent conformers are taken from the crystal into isolation with fixed geometries, the molecule of the β-form is also energetically the most favored, whereas geometry optimization with fixed C–Te–Te–C angle leads to a slightly lower energy for the γ-form (Figure 13). Moreover, our experimental investigations indicate that the α-form becomes thermodynamically stable at room-temperature, because from all of our crystallization experiments there is no hint for the formation of traces of the other two polymorphic modifications and our thermo-analytical measurements do not show any polymorphic transformation.

Consequently, one must assume that the α- and the β-form are related by enantiotropism, which means that the free energy-temperature curves will cross at the thermodynamic transition temperature, where the β-form can transform endothermically into the α-form. If the γ-form is related to the other forms by monotropism or enantiotropism, we do not know. Unfortunately, because no rational access to larger amounts of the other two modifications were found we cannot prove their exact

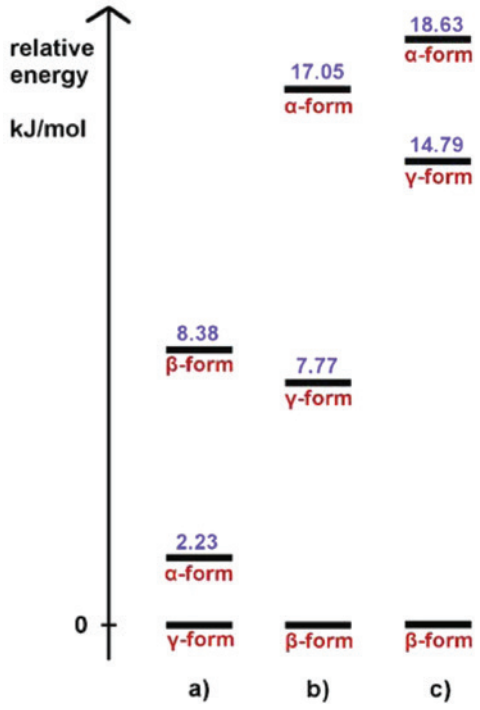

Fig. 13: (a) Relative energies of the isolated conformers with optimized geometry at constrained C–Te–Te–C angle. (b) Relative energies of the isolated conformers with experimental geometry. (c) Cohesive energies from fully periodic calculations taking BSSE corrections into account.

thermodynamic relations. To this end, the β-and the γ-form must remain "disappearing polymorphs" [47, 48].

Experimental and computational details

Experimental details

Differential scanning calorimetry: DSC investigations were performed with the DSC 204/1/F from Netzsch and the DSC 1 Star System with STARe Excellence Software from Mettler-Toledo AG. The measurements were performed in Al pans with different heating rates under nitrogen. The instruments were calibrated using standard reference materials.

Differential thermal analysis and thermogravimetry: DTA-TG measurements were performed in Al_2O_3 crucibles using a STA-409CD thermobalance from Netzsch. Several measurements under nitrogen atmosphere (purity 5.0) with different heating rates were performed. All measurements were performed with a flow rate of 75 mL/min and were corrected for buoyancy and current effects.

Powder X-ray diffraction experiments: X-ray powder diffraction experiments were performed using a STOE STADI P transmission powder diffractometer using CuKα radiation, that is equipped with an Mythen K1 detector.

Single-crystal X-ray diffraction experiments: Intensity data of the β-form and the γ-form of $(2,6\text{-}Mes_2C_6H_3Te)_2$ were collected on a Siemens P4 diffractometer with graphite-monochromated Mo-Kα (0.7107 Å) radiation. Data was reduced and empirically corrected for absorption [66]. The structure was solved by direct methods and difference Fourier synthesis with subsequent full-matrix least-squares refinements on F^2, using all data [67]. All non-hydrogen atoms were refined using anisotropic displacement parameters. Hydrogen atoms were included in geometrically calculated positions using a riding model. Crystal and refinement data are collected in Table 1. Figures were created using DIAMOND [68]. Crystallographic data for the structural analysis have been deposited with the Cambridge Crystallographic Data Centre. Copies of this information may be obtained free of charge from The Director, CCDC, 12 Union Road, Cambridge CB2 1EZ, UK (Fax: +44-1223-336033; e-mail: deposit@ccdc.cam.ac.uk or http://www.ccdc.cam.ac.uk) under the deposition numbers 651206, 1823140 and 1823141.

Computational details

All isolated-molecule calculations were carried out with the program Gaussian09 [69], and the DFT functional B3PW91, which has previously been used successfully for tellurium chemistry [70]. The effective-core potential basis set LANL2DZDP was adopted for Te [71]; for C and H, the basis set 6-31G(d,p) was used. Except where we explicitly wanted to test the effect of neglecting dispersion on the optimized geometry, the Grimme-type D3BJ empirical dispersion correction method was employed [72]. A conductor-like screening model (COSMO) [58] was tested in an additional calculation to check the influence of the solvent acetonitrile on the optimized geometry. Frequency analyses were carried out to ensure a minimum on the potential energy surface. In those cases, where a negative frequency occurred that did not involve the Menshutkin interactions or the C–Te–Te–C region, where a finer integration grid or tighter convergence criteria did not prevent the occurrence of the negative frequency, and where it was smaller than an absolute value of 5 cm^{-1}, it was neglected and the resulting geometry used for further analysis. Free geometry optimizations were started from each of the experimental geometries of the α-, β- and γ-form, and always yielded the same potential energy minimum. Further geometry optimizations from the same starting geometries involved fixing the C–Te–Te–C angle to the values from experiment upon relaxing all other degrees of freedom. For the model compound Me–Te–Te–Me, a relaxed potential energy surface scan upon variation of the C–Te–Te–C angle in 5° intervals was carried out with the same method and basis set. Based on the Gaussian isolated-molecule calculations, a topological analysis according to the Quantum Theory of Atoms in Molecules (QTAIM) [53] was carried out and visualized with the software AIMAll [73]. The non-covalent index (NCI) was calculated with the software NCIMilano [74] and visualized with the program Moliso [75]. The Electron Localizability Indicator (ELI-D) [54, 55] was calculated with DGrid 5.0 [76] and also visualized as an isosurface representation with Moliso.

In addition to the Gaussian calculations, Crystal14 [77] was used to calculate cohesive energies. To adjust the calculations to the

solid-state boundary conditions, slightly different methods and basis sets had to be used. The method B3LYP-D2 was used, the only dispersion corrected method in Crystal14 [78], the effective core basis set m-pVDZ-PP for the Te atoms [79], and the basis set 6-311G(d,p) for C and H atoms. First, the energies of the isolated molecules were calculated at the fixed experimental geometries of the α-, β- and γ-form with C–H bond distances elongated to averaged values from neutron diffraction as given in the literature [80]; second, the energies of the unit cells of α, β and γ-form were derived at a fully periodic level at the fixed C–H elongated experimental geometries of the crystals. Third, the basis set superposition error (BSSE) [81] was determined and accounted for in the calculation of the cohesive energies. As an approximation to the cohesive energy, the sum of dimeric interaction energies in the crystal structures of α, β and γ-form were calculated with Gaussian09 [69] and Tonto [82] inside Crystal Explorer 17 [83] using the default protocol and default benchmarked theoretical level B3LYP/6-31G(d,p) for C and H atoms as well as DGDZVP for Te atoms. The total interaction energy per dimer is the scaled sum of electrostatic, dispersion, polarization and exchange-repulsion terms [59, 60]. Crystal Explorer 17 [83] was also used for the calculation and visualization of Hirshfeld surfaces and fingerprint plots [28].

Acknowledgment: The Deutsche Forschungsgemeinschaft (DFG) is gratefully acknowledged for financial support (Emmy Noether program GR 4451/1-1). We thank Bartolomeo Civalleri (University of Turin) and Gabriele Saleh (Trinity College Dublin) for their help with Crystal14 and NCIMilano. Simon Grabowsky is indebted to Peter Luger for his generous support and mentoring. All of us salute him for his outstanding career in science pioneering modern crystallography.

References

[1] D. Barga, F. Grepioni, L. Maini, *Chem. Commun*. **2010**, *46*, 6232.
[2] P. Hobza, K. Müller-Dethlefs, *Non-Covalent Interactions: Theory and Experiment*, Royal Society of Chemistry, Cambridge, UK, **2010**.
[3] K. Müller-Dethlefs, P. Hobza, *Chem. Rev*. **2000**, *100*, 143.
[4] J. D. Dunitz, *IUCrJ* **2015**, *2*, 157.
[5] J. D. Dunitz, A. Gavezzotti, *Angew. Chem. Int. Ed*. **2005**, *44*, 1766.
[6] C. Lecomte, E. Espinosa, C. F. Matta, *IUCrJ* **2015**, *2*, 161.
[7] T. S. Thakur, R. Dubey, G. R. Desiraju, *IUCrJ* **2015**, *2*, 159.
[8] A. Gavezzotti, *New J. Chem*. **2016**, *40*, 6848.
[9] C. F. Matta, J. Hernández-Trujillo, T. H. Tang, R. F. W. Bader, *Chem. Eur. J*. **2003**, *9*, 1940.
[10] J. Poater, M. Solà, F. M. Bickelhaupt, *Chem. Eur. J*. **2006**, *12*, 2889.
[11] J. Echeverría, G. Aullón, D. Danovich, S. Shaik, S. Alvarez, *Nature Chem*. **2011**, *3*, 323.
[12] S. Rösel, H. Quanz, C. Logemann, J. Becker, E. Mossou, L. Cañadillas-Delgado, E. Caldeweyher, S. Grimme, P. R. Schreiner, *J. Am. Chem. Soc*. **2017**, *139*, 7428.
[13] D. J. Liptrot, P. P. Power, *Nat. Rev. Chem*. **2017**, *1*, 0004.
[14] J. P. Wagner, P. R. Schreiner, *Angew. Chem. Int. Ed*. **2015**, *54*, 12274.
[15] J.-D. Guo, D. J. Liptrot, S. Nagase, P. P. Power, *Chem. Sci*. **2015**, *6*, 6235.
[16] J. P. Wagner, P. R. Schreiner, *J. Chem. Theory Comput*. **2016**, *12*, 231.
[17] R. Pal, S. Mebs, M. W. Shi, D. Jayatilaka, J. M. Krzeszczakowska, L. A. Malaspina, M. Wiecko, P. Luger, M. Hesse, Y.-S. Chen, J. Beckmann, S. Grabowsky, *Inorg. Chem*. **2018**, *122*, 3665.
[18] J. Bernstein, A. T. Hagler, *J. Am. Chem. Soc*. **1978**, *100*, 673.
[19] A. Nangia, *Acc. Chem. Res*. **2008**, *5*, 595.
[20] D. Barga, F. Grepioni, *Chem. Soc. Rev*. **2000**, *29*, 229.
[21] J. Bernstein, *Polymorphism in Molecular Crystals*, Oxford University Press, Oxford, UK, **2002**.
[22] J. Bernstein, *Cryst. Growth. Des*. **2011**, *11*, 632.
[23] A. J. Cruz-Cabeza, J. Bernstein, *Chem. Rev*. **2014**, *114*, 2170.
[24] A. I. Kitaigorodskii, *Adv. Struct. Res. Diffr. Methods* **1970**, *3*, 173.
[25] A. I. Kitaigorodsky, *Molecular Crystals and Molecules*, Academic Press, New York, London, **1973**.
[26] J. J. McKinnon, A. S. Mitchell, M. A. Spackman, *Chem. Eur. J*. **1998**, *4*, 2136.
[27] M. A. Spackman, *Phys. Scr*. **2013**, *87*, 048103.
[28] M. A. Spackman, D. Jayatilaka, *CrystEngComm* **2009**, *11*, 19.
[29] J. J. McKinnon, F. P. A. Fabbiani, M. A. Spackman, *Cryst. Growth Des*. **2007**, *7*, 755.
[30] L. Mazur, A. E. Koziol, K. N. Jarzembska, R. Paprocka, B. Modzelewska-Banachiewicz, *Cryst. Growth Des*. **2017**, *17*, 2104.
[31] H. Schmidbaur, A. Schnier, *Organometallics* **2008**, *27*, 2361.
[32] J. Zukerman-Schpector, I. Haiduc, *CrystEngComm*. **2002**, *4*, 178.
[33] E. R. T. Tiekink, J. Zukerman-Schpector, *CrystEngComm* **2009**, *11*, 2701.
[34] R. Lo, P. Švec, Z. Růžičková, A. Růžička, R. Hobza, *Chem. Commun*. **2016**, *52*, 3500.
[35] J. Beckmann, M. Hesse, H. Poleschner, K. Seppelt, *Angew. Chem. Int. Ed*. **2007**, *46*, 8277.
[36] J. Beckmann, P. Finke, S. Heitz, M. Hesse, *Eur. J. Inorg. Chem*. **2008**, 1921.
[37] J. Beckmann, P. Finke, M. Hesse, B. Wettig, *Angew. Chem. Int. Ed*. **2008**, *47*, 9982.
[38] J. Beckmann, J. Bolsinger, P. Finke, M. Hesse, *Angew. Chem. Int. Ed*. **2010**, *49*, 8030.
[39] O. Mallow, M. A. Khanfar, M. Malischewski, P. Finke, M. Hesse, E. Lork, T. Augenstein, F. Breher, J. R. Harmer, N. V. Vasilieva, A. Zibarev, A. S. Bogomyakov, K. Seppelt, J. Beckmann, *Chem. Sci*. **2015**, *6*, 497.
[40] J. Beckmann, J. Bolsinger, S. Mebs, *Main Group Met. Chem*. **2013**, *36*, 57 and references cited.
[41] D. J. Sandman, L. Li, S. Tripathy, J. C. Stark, L. A. Acampora, B. M. Foxman, *Organometallics* **1994**, *13*, 348.
[42] F. H. Kruse, R. E. Marsh, J.D. McCullough, *Acta Crystallogr.* **1957**, *10*, 201.
[43] G. Van den Bossche, M. R. Spirlet, O. Dideberg, L. Dupont, *Acta Crystallogr.* **1984**, *C40*, 1011.
[44] G. Llabres, M. Baiwir, J. L. Piette, *J. Appl. Crystallogr.* **1974**, *7*, 299.
[45] M. R. Spiret, G. van den Bossche, O. Dideberg, L. Dupont, *Acta Crystallogr.* **1979**, *B35*, 1727.

[46] M. J. Turner, J. J. McKinnon, D. Jayatilaka, M. A. Spackman, *CrystEngComm* **2011**, *13*, 1804.
[47] J. D. Dunitz, J. Bernstein, *Acc. Chem. Res*. **1995**, *28*, 193.
[48] D.-K. Bučar, R. W. Lancaster, J. Bernstein, *Angew. Chem. Int. Ed*. **2015**, *54*, 6972.
[49] T. Threlfall, *Org. Proc. Res. Dev*. **2003**, *7*, 1017.
[50] A. L. Fuller, A. S. Scott-Hayward, Y. Li, M. Bühl, A. M. Z. Slawin, J. D. Woollins, *J. Am. Chem. Soc*. **2010**, *132*, 5799.
[51] W.-W. du Mont, L. Lange, H. H. Karsch, K. Peters, E. M. Peters, H. G. von Schnering, *Chem. Ber*. **1988**, *121*, 11.
[52] S. Salehzadeh, M. Saberinasab, *Mol. Phys*. **2016**, *114*, 3669.
[53] R. F. W. Bader, *Atoms in Molecules: A Quantum Theory*, Cambridge University Press, Oxford, UK, **1991**.
[54] E. R. Johnson, S. Keinan, P. Mori-Sánchez, J. Contreras-Garciá, A. J. Cohen, W. Yang, *J. Am. Chem. Soc*. **2010**, *132*, 6498.
[55] J. Contreras-Garciá, R. A. Boto, F. Izquierdo-Ruiz, I. Reva, T. Woller, M. Alonso, *Theor. Chem. Acc*. **2016**, *135*, 242.
[56] M. Kohout, *Int. J. Quantum Chem*. **2004**, *97*, 651.
[57] M. Kohout, F. R. Wagner, Y. Grin, *Theor. Chem. Acc*. **2008**, *119*, 413.
[58] A. Klamt, G. J. Schüürmann, *J. Chem. Soc. Perkin Trans 2*, **1993**, 799.
[59] M. J. Turner, S. Grabowsky, D. Jayatilaka, M. A. Spackman, *J. Phys. Chem. Lett*. **2014**, *5*, 4249.
[60] C. F. Mackenzie, P. R. Spackman, D. Jayatilaka, M. A. Spackman, *IUCrJ* **2017**, *4*, 575.
[61] S. P. Thomas, P. R. Spackman, D. Jayatilaka, M. A. Spackman, *J. Chem. Theory Comput*. **2018**, *14*, 1614.
[62] S. P. Thomas, M. A. Spackman, *Aust. J. Chem*. **2018**, *71*, 279.
[63] M. A. Spackman, P. G. Byrom, *Chem. Phys. Lett*. **1997**, *267*, 215.
[64] J. J. McKinnon, D. Jayatilaka, M. A. Spackman, *Chem. Commun*. **2007**, 3814.
[65] The energies calculated to investigate the thermodynamics of the systems in this paper refer to zero Kelvin. At zero Kelvin, entropy can be neglected for the free energy according to $\Delta G = \Delta H - T\Delta S$. However, to get some insight into the entropy based on the experimental geometries, we have estimated the entropies using a method by A. Ø. Madsen, S. Larsen, *Angew. Chem. Int. Ed*. **2007**, *46*, 8609, that was applied successfully, e.g. in: R. Pal, M. B. M. Reddy, B. Dinesh, P. Balaram, T. N. Guru Row, *J. Phys. Chem. A* **2014**, *118*, 9568. Normal-mode frequencies were estimated using a TLS analysis inside the program thma11 at the temperature of the diffraction experiment (173 K). For every normal-mode frequency value, an entropy is calculated upon projection to room temperature, and then summed up over all modes for a total entropy estimate of the crystal. Here, the β-form has the lowest entropy (167.55 J mol^{-1} K^{-1}), but very similar to the γ-form (167.81 J mol^{-1} K^{-1}), whereas the α-form has a significantly higher entropy (173.12 J mol^{-1} K^{-1}).
[66] N. Walker, D. Stuart, *Acta Crystallogr*. **1983**, *A39*, 158.
[67] O. V. Dolomanov, L. J. Bourhis, R. J. Gildea, J. A. K. Howard, H. Puschmann, *J. Appl. Crystallogr*. **2009**, *42*, 339.
[68] K. Brandenburg, H. Putz, H. DIAMOND V3.1d, Crystal Impact GbR, **2006**.
[69] Gaussian 09, Revision D.01, M. J. Frisch, G. W. Trucks, H. B. Schlegel, G. E. Scuseria, M. A. Robb, J. R. Cheeseman, G. Scalmani, V. Barone, B. Mennucci, G. A. Petersson, H. Nakatsuji, M. Caricato, X. Li, H. P. Hratchian, A. F. Izmaylov, J. Bloino, G. Zheng, J. L. Sonnenberg, M. Hada, M. Ehara, K. Toyota, R. Fukuda, J. Hasegawa, M. Ishida, T. Nakajima, Y. Honda, O. Kitao, H. Nakai, T. Vreven, J. A. Montgomery, Jr., J. E. Peralta, F. Ogliaro, M. Bearpark, J. J. Heyd, E. Brothers, K. N. Kudin, V. N. Staroverov, R. Kobayashi, J. Normand, K. Raghavachari, A. Rendell, J. C. Burant, S. S. Iyengar, J. Tomasi, M. Cossi, N. Rega, J. M. Millam, M. Klene, J. E. Knox, J. B. Cross, V. Bakken, C. Adamo, J. Jaramillo, R. Gomperts, R. E. Stratmann, O. Yazyev, A. J. Austin, R. Cammi, C. Pomelli, J. W. Ochterski, R. L. Martin, K. Morokuma, V. G. Zakrzewski, G. A. Voth, P. Salvador, J. J. Dannenberg, S. Dapprich, A. D. Daniels, Ö. Farkas, J. B. Foresman, J. V. Ortiz, J. Cioslowski, D. J. Fox, Gaussian, Inc., Wallingford CT, **2010**.
[70] O. Mallow, J. Bolsinger, P. Finke, M. Hesse, Y.-S. Chen, A. Duthie, S. Grabowsky, P. Luger, S. Mebs, J. Beckmann, *J. Am. Chem. Soc*. **2014**, *136*, 10870.
[71] D. Feller, *J. Comp. Chem*. **1996**, *17*, 1571.
[72] S. Grimme, S. Ehrlich, L. Goerigk, *J. Comp. Chem*. **2011**, *32*, 1456.
[73] T. A. Keith, AIMAll (Version 15.05.18), TK Gristmill Software, Overland Park KS, USA, 2015 (http://aim.tkgristmill.com).
[74] G. Saleh, L. Lo Presti, C. Gatti, D. Ceresoli, *J. Appl. Crystallogr*. **2013**, *46*, 1513.
[75] C. B. Hübschle, P. Luger, *J. Appl. Crystallogr*. **2006**, *39*, 901.
[76] M. Kohout, DGrid, version 4.6. Radebeul, Germany, **2011**.
[77] R. Dovesi, R. Orlando, A. Erba, C. M. Zicovich-Wilson, B. Civalleri, S. Casassa, L. Maschio, M. Ferrabone, M. De La Pierre, P. D'Arco, Y. Noël, M. Causà, M. Rérat, B. Kirtman, *Int. J. Quantum Chem*. **2014**, *114*, 1287.
[78] C. Bartolomeo, C. M. Zicovich-Wilson, L. Valenzano, P. Ugliengo, *CrystEngComm* **2008**, *10*, 405.
[79] J. Heyd, J. E. Peralta, G. E. Scuseria, R. L. Martin, *J. Chem. Phys*. **2005**, *123*, 174101.
[80] F. H. Allen, I. J. Bruno, *Acta Crystallogr. B* **2010**, *66*, 380.
[81] S. F. Boys, F. Bernardi, *Mol. Phys*. **1970**, *19*, 553.
[82] D. Jayatilaka, D. J. Grimwood, *Tonto: A Fortran Based Object-Oriented System for Quantum Chemistry and Crystallography*, Springer, New York, **2003**.
[83] M. J. Turner, J. J. McKinnon, S. K. Wolff, D. J. Grimwood, P. R. Spackman, D. Jayatilaka, M. A. Spackman, CrystalExplorer17, University of Western Australia, **2017**. http://hirshfeldsurface.net.

Supplementary Material: The online version of this article offers supplementary material (https://doi.org/10.1515/zkri-2018-2077).